2018 IEEE/RSJ International Conference on Intelligent Robots and Systems (IROS)
Madrid, Spain, October 1-5, 2018

Rendering of Virtual Volumetric Shapes Using an Electromagnetic-Based Haptic Interface

Alaa Adel*†, Mina M. Micheal*†, Mohamed Abou Seif*, Slim Abdennadher* and Islam S. M. Khalil*

***Abstract*— Mid-Air haptic devices have become an active area of research because of their potential impact to augmented/virtual reality. In this work, we develop an electromagnetic-based haptic interface to provide controlled magnetic forces on a wearable orthopedic finger splint with a single magnetic dipole. We model the electromagnetic forces exerted on the finger splint, optimize the design of the electromagnetic coils, and develop an impedance-type haptic rendering algorithm using position feedback. This rendering algorithm capitalizes on minimizing the error between the exerted magnetic force and the desired constraint force of a virtual three-dimensional (3D) object based on the position of the finger splint. In order to investigate the influence of incorporating position feedback, we conduct a comparative study for the same group of participants with (Case I) and without (Case II) position feedback. Our experimental results show that position feedback enables participants to achieve success rate of $66.87 \pm 15.0\%$ $(n = 160)$ in distinguishing between the geometry of four 3D virtual objects. This rate is decreased to $55.15 \pm 15.8\%$ $(n = 160)$ in the absence of position feedback. Our analysis shows statistical evidence to conclude that the mean success rate for Case I is greater than that of Case II, at $\alpha = 0.1$ and 90% confidence level.**

I. Introduction

There has been a considerable progress in augmented/virtual reality (AR/VR) technologies owing to their potential in several applications such as medical simulation training, education, and video game industry. A basic feature for any of these applications is to provide the operator with the ability to interact and explore virtual objects with minimal contact and interaction. This requirement can be met by integrating haptic and AR/VR technologies [1], [2]. A basic haptic system architecture consists mainly of a virtual environment, a haptic rendering algorithm, and a haptic device which maps the force signal from the computer into a force that the operator can perceive [3], as shown in Fig. 1. These haptic systems are classified based on the triggered sense into tactile and kinesthetic haptic devices. The former stimulate the receptors located on the skin, while the latter provides direct interaction through active surfaces and mid-air devices (without direct contact). Therefore, mid-air devices are suitable for AR/VR ecosystems [4]. Several research groups have developed mid-air haptic devices based on forces generated at a distance using acoustic radiation pressure [5], air pressure [6], [7], and magnetic field gradient [8]. Zhang *et al.* have proposed a magnetic system for rendering volumetric shapes in mid-air. They have designed and simulated the rendering process of virtual shapes using the magnetic forces exerted on a magnetic dipole without position feedback [8]. In our previous study [9], we have demonstrated the ability to generate controlled magnetic forces on a wearable orthopedic finger splint without position feedback. The implication is that any movement away from a pre-defined constraint surface of the 3D virtual object would decrease the ability of the operator to perceive its features, and as a consequence, the ability of the participants to distinguish between different geometries has not been statistically significant. Here we develop an electromagnetic-based haptic interface for rendering 3D virtual objects and design an impendence-type haptic rendering algorithm using position feedback, and achieve the following:

- Modeling of the force exerted on a dipole under the influence of a controlled external magnetic field;
- Optimization of the parameters of the electromagnetic coils to obtain force in excess of 2 N at height of 3 cm;
- Development of an impedance-type haptic rendering algorithm for 3D virtual objects;
- Experimental investigation on the ability of participants to differentiate between 3D virtual objects.

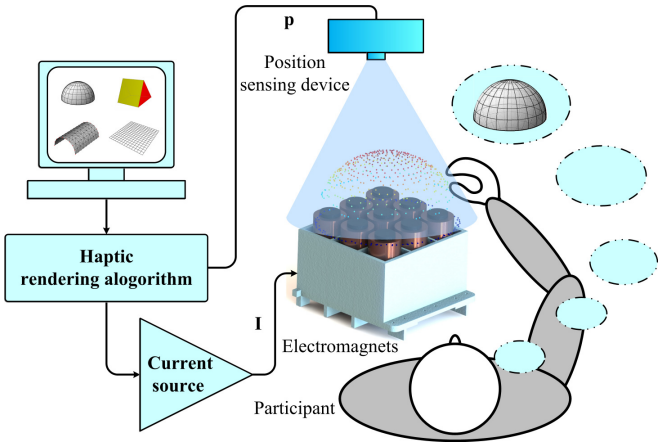

Fig. 1. Magnetic rendering of virtual objects in mid-air enables a participant to distinguish the features of three-dimensional (3D) virtual objects. The magnetic rendering is achieved using an electromagnetic-based haptic interface. This interface consists of an array of electromagnetic coils, a wearable orthopedic finger splint with a single magnetic dipole moment, and an impendence-type haptic rendering algorithm. Each coil is powered independently using a current source. A current input ($\mathbf{I} \in \mathbf{R}^{9\times1}$) is provided to the coils based on the geometry of the object and the position ($\mathbf{p} \in \mathbf{R}^{3\times1}$) of the participant. The system exerts a controlled magnetic force based on the geometry of the 3D virtual objects and observations of participants are used to evaluate the system.

This work was supported by the DAAD-BMBF funding project and the Science and Technology Development Fund in Egypt (No. 23016).

*The authors are with the German University in Cairo, New Cairo, Egypt.
†These authors contributed equally to this work.

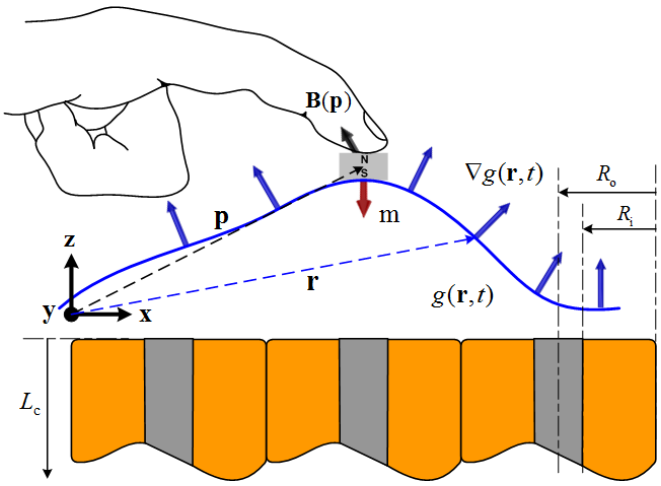

Fig. 2. The constraint surface $g(\mathbf{r}, t)$ of the virtual object (blue curve) provides a constraint force $\nabla g(\mathbf{r}, t)$. Magnetic field $\mathbf{B}(\mathbf{p})$ at a point $\mathbf{p}$ exerts a magnetic force on the magnetic dipole $\mathbf{m}$. This magnetic dipole is attached to the operator via an orthopedic finger splint, and its position is measured using a position sensing device. The variables R_i, R_o, and L_c represent the inner-diameter, outer-diameter, and length of the coil, respectively. $\mathbf{r}$ is the position of a point on the constraint surface.

The remainder of this paper is organized as follows: Section II provides insights into the modeling of the magnetic forces and descriptions pertaining to our electromagnetic-based haptic interface. Design details are provided in Section II. Section III presents our experimental results and investigations using statistical analysis. Finally, Section IV concludes and provides directions for future work.

II. Design and Development of the Electormagnetic-Based Haptic Device

Magnetic rendering of a 3D virtual object is achieved using magnetic forces exerted on the dipole of an orthopedic finger splint. The magnetic and constraint forces are modeled and used in the design of this system.

A. Modeling of the Magnetic and Constraint Forces

Magnetic fields are generated using an in-plane array of m electromagnetic coils. We apply controlled magnetic force on the finger splint (Fig. 2) with a single magnetic dipole moment ($\mathbf{m} \in \mathbf{R}^{3\times1}$) using a controlled magnetic field $\mathbf{B}(\mathbf{p}) \in \mathbf{R}^{3\times1}$. Let $\mathbf{p} \in \mathbf{R}^{3\times1}$ be the position of the permanent magnet attached to the finger splint. If a controlled magnetic field is applied using a configuration of planar electromagnetic coils then a magnetic force ($\mathbf{F} \in \mathbf{R}^{3\times1}$) is generated and given by

$$\mathbf{F} = \nabla(\mathbf{m} \cdot \mathbf{B}(\mathbf{p})). \tag{1}$$

The magnetic force components F_x, F_y, and F_z in (1) are calculated using

$$\begin{bmatrix} F_x \\ F_y \\ F_z \end{bmatrix} = \begin{bmatrix} \frac{\partial B_x(\mathbf{p})}{\partial x} & \frac{\partial B_y(\mathbf{p})}{\partial x} & \frac{\partial B_z(\mathbf{p})}{\partial x} \\ \frac{\partial B_x(\mathbf{p})}{\partial y} & \frac{\partial B_y(\mathbf{p})}{\partial y} & \frac{\partial B_z(\mathbf{p})}{\partial y} \\ \frac{\partial B_x(\mathbf{p})}{\partial z} & \frac{\partial B_y(\mathbf{p})}{\partial z} & \frac{\partial B_z(\mathbf{p})}{\partial z} \end{bmatrix} \begin{bmatrix} m_x \\ m_y \\ m_z \end{bmatrix}, \tag{2}$$

where m_x, m_y, and m_z are the components of the magnetic dipole moment of the permanent magnet, and $B_x(\mathbf{p})$, $B_y(\mathbf{p})$, and $B_z(\mathbf{p})$ are the components of the external magnetic field along $\mathbf{x}$-, $\mathbf{y}$-, and $\mathbf{z}$-axis, respectively. These components are mapped onto current input as follows:

$$\begin{bmatrix} F_x \\ F_y \\ F_z \end{bmatrix} = \begin{bmatrix} \frac{\partial \widetilde{\mathbf{B}}_x(\mathbf{p})\mathbf{I}}{\partial x} & \frac{\partial \widetilde{\mathbf{B}}_y(\mathbf{p})\mathbf{I}}{\partial x} & \frac{\partial \widetilde{\mathbf{B}}_z(\mathbf{p})\mathbf{I}}{\partial x} \\ \frac{\partial \widetilde{\mathbf{B}}_x(\mathbf{p})\mathbf{I}}{\partial y} & \frac{\partial \widetilde{\mathbf{B}}_y(\mathbf{p})\mathbf{I}}{\partial y} & \frac{\partial \widetilde{\mathbf{B}}_z(\mathbf{p})\mathbf{I}}{\partial y} \\ \frac{\partial \widetilde{\mathbf{B}}_x(\mathbf{p})\mathbf{I}}{\partial z} & \frac{\partial \widetilde{\mathbf{B}}_y(\mathbf{p})\mathbf{I}}{\partial z} & \frac{\partial \widetilde{\mathbf{B}}_z(\mathbf{p})\mathbf{I}}{\partial z} \end{bmatrix} \begin{bmatrix} m_x \\ m_y \\ m_z \end{bmatrix}, \tag{3}$$

where $\widetilde{\mathbf{B}}_x(\mathbf{p})$, $\widetilde{\mathbf{B}}_y(\mathbf{p})$ and $\widetilde{\mathbf{B}}_z(\mathbf{p})$ are the magnetic field current mappings at a point $\mathbf{p}$ of the field components along $\mathbf{x}$-, $\mathbf{y}$- and $\mathbf{z}$-axis, respectively. The magnetic force component F_z along $\mathbf{z}$-axis is responsible for rendering the geometry of the virtual object and given by

$$F_z = \frac{\partial \widetilde{\mathbf{B}}_x(\mathbf{p})\mathbf{I}}{\partial z} m_x + \frac{\partial \widetilde{\mathbf{B}}_y(\mathbf{p})\mathbf{I}}{\partial z} m_y + \frac{\partial \widetilde{\mathbf{B}}_z(\mathbf{p})\mathbf{I}}{\partial z} m_z. \tag{4}$$

The components of the magnetic dipole moment along $\mathbf{x}$- and $\mathbf{y}$-axis (m_x and m_y) are relatively smaller than m_z. Therefore, we use the superposition principle [10], [11] and simplify (4) as follows:

$$F_\mathrm{t} = \frac{\partial}{\partial z} \left(\sum_{i=1}^{m} \widetilde{\mathbf{B}}_{z_i}(\mathbf{p}) I_i \right) m_z. \tag{5}$$

where F_t is the total magnetic force exerted on the magnetic dipole. Further, I_i and $\widetilde{\mathbf{B}}_{z_i}$ are the ith current input and the ith field-current map, respectively.

Now we turn our attention to the surface constraint force of the virtual object that provides constraint surface $g(\mathbf{r}, t) = 0$, where $\mathbf{r} \in \mathbf{R}^{3\times1}$ is the position of a point on the constraint surface. Therefore, the constraint surface results in a constraint force $\mathbf{f}$ that lays perpendicular to the surface and is given by

$$\mathbf{f} = \lambda h(x, y), \tag{6}$$

where $h(x, y)$ is the height map of the virtual shape and λ is a force constant. We define the following error function $(e(\mathbf{I}))$ between the required magnetic force $\mathbf{f}$ and the controlled magnetic force F_t using (5) and (6):

$$e(\mathbf{I}) = \mathbf{f} - \frac{\partial}{\partial z} \left(\sum_{i=1}^{m} \widetilde{\mathbf{B}}_{z_i}(\mathbf{p}) I_i \right) m_z. \tag{7}$$

Our objective is to find the optimal current that minimizes the error between the required magnetic force and the controlled magnetic force. Therefore, we use (7) to formulate the following optimization objective function:

$$\begin{aligned} \underset{\mathbf{I}}{\text{minimize}} \quad & \epsilon(\mathbf{I}) = ||e(\mathbf{I})|| \\ \text{subject to} \quad & 0 < I_i \leq u_i, \quad i = 1, \ldots, m, \\ & \sum_{i=1}^{m} I_i \leq I_\mathrm{t}, \quad i = 1, \ldots, m. \end{aligned} \tag{8}$$

In (8), $\epsilon(\mathbf{I})$ is a scalar objective function to be minimized using I. Further, u_i is an upper-limit on the input current and I_t is the maximum current provided via a power source.

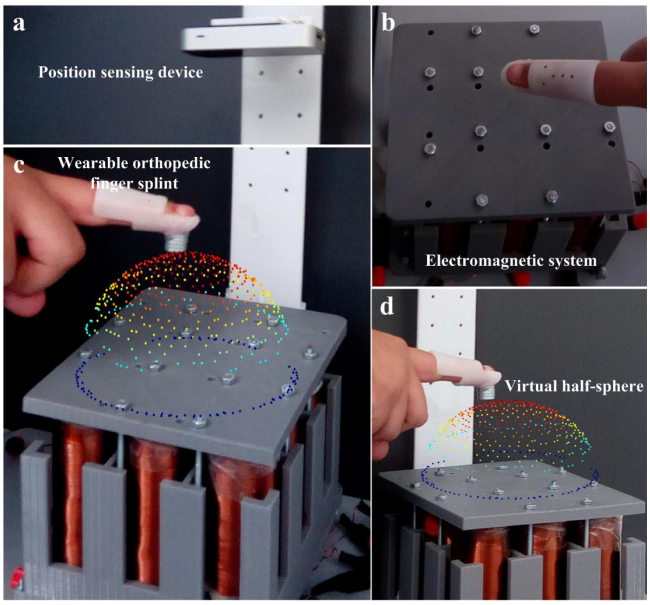

Fig. 3. An electromagnetic-based haptic interface enables the operator to interact with virtual objects in three-dimensional (3D) space. (a) A position sensing device is used to measure the position of the wearable finger splint in 3D space. (b) Position of the wearable finger splint is fed back to the control system to exert a magnetic force based on the rendered geometry. (c) Magnetic rendering of half-sphere is achieved and participants distinguish its features with success rate of 67.5%. (d) Participants distinguish this geometry in 65 seconds. *Please refer to the accompanying video.*

Therefore, equation (8) adapts the input currents simultaneously to exert a magnetic force on the user's finger. In (6), the force constant λ controls the values of the constraint forces. In case of selecting relatively large values for λ, for which $\mathbf{f}$ is relatively large, an increase in the force error (7) can result in relatively large current inputs that are not viable due to the constraints in (8). On the other hand, the ability of the operator to perceive the virtual shape is decreased for relatively small values of the force constant λ. Therefore, we define an error function that represents the mean squared error between the constraint forces and the generated magnetic force

$$e(\lambda, \mathbf{I}) = \frac{1}{n}\sum_{j=1}^{n} \|\lambda h(x_j, y_j) - \sum_{i=1}^{m} I_i \frac{\partial \widetilde{\mathbf{B}}_{z_i}(\mathbf{p})}{\partial z} m_z\|^2, \quad (9)$$

where n is the number of points on the constraint surface of the virtual object. Equation (9) is used in the following optimization problem:

$$\begin{aligned} \max_{\lambda} \min_{\mathbf{I}} \quad & e(\lambda, \mathbf{I}) \\ \text{subject to} \quad & 0 < I_i \leq u_i, \quad i = 1, \ldots, m, \\ & \sum_{i=1}^{m} I_i \leq I_{\mathrm{t}}, \quad i = 1, \ldots, m. \end{aligned} \quad (10)$$

This optimization is solved only once for each 3D virtual object to obtain λ and during the rendering process (8) is used to generate the required current input.

B. Electromagnetic-Based Haptic Interface

The electromagnetic-based haptic interface (Fig. 3) consists of an array ($m = 9$) of electromagnetic coils that generates magnetic forces on a Neodymium permanent magnet (S-10-05-N, N52, nickel-plated, supermanete, Gottmadingen, Germany) with axial magnetization of 1.1579×10^{6} A.m^{-1} and rated current of 2 A. The thickness and diameter of the permanent magnet are 10 mm and 10 mm, respectively. This magnet is attached to the tip of a wearable finger splint, and enables the user to perceive the magnetic force. The minimum force of our sensory range is approximately 0.8 mN [2]. Therefore, we optimize the design of the electromagnetic coils to satisfy this criterion. The distance between the magnet and the coils is fixed to 30 mm and the wire diameter is constant with diameter of 0.7 mm. The inner- and outer-diameter of the coil, and its length are optimized using

$$\begin{aligned} \underset{R_{\mathrm{i}}, R_{\mathrm{o}}, L_{\mathrm{c}}}{\text{maximize}} \quad & F = m_z \frac{\partial B_z}{\partial z}(R_{\mathrm{i}}, R_{\mathrm{o}}, L_{\mathrm{c}}) \\ \text{subject to} \quad & R_{\mathrm{c}} < 6 \quad , \quad 5\tau < 100, \\ & R_{\mathrm{o}} < R_{\max} \quad , \quad L_{\mathrm{c}} < L_{\max}. \end{aligned} \quad (11)$$

where m_z is the dipole moment of the magnet and $\frac{\partial B_z}{\partial z}(R_{\mathrm{i}}, R_{\mathrm{o}}, L_{\mathrm{c}})$ is the gradient of the magnetic field with respect to the vertical direction. Further, R_{i} and R_{o} are the inner- and outer-diameter of the coil, respectively, and L_c is the length of the coil. This optimization problem provides optimal R_{i}, R_{o}, and L_{c} to maximize the generated force along $\mathbf{z}$-axis. The first constraint limits the resistance of the coil below 6 Ω to enable the coil to draw approximately 6 A (coils are supplied with 36 V). The second constraint provides the time response of the coil $\tau = \frac{L_{\mathrm{c}}}{R_{\mathrm{c}}}$, where L_{c} and R_{c} are its inductance and resistance, respectively. The coil reaches its steady-state in approximately 100 ms. The third and fourth constraints define the maximum outer-diameter $R_{\max}$ and length $L_{\max}$ of each coil.

The optimization is performed using MATLAB's *fmincon* function. This optimization routine is solved iteratively using interior-method for constrained non-linear optimization and we obtain maximum force of 780 mN while satisfying the constraints given by (8). Each electromagnetic coil has inner- and outer-diameters of 24 mm and 38 mm, respectively. The height of the coil and the length of its low carbon steel core are 100 mm and 110 mm, respectively. The number of turns is 1429. Each of the electromagnets is independently supplied with current using electric drivers (MD10C, Cytron Technologies Sdn. Bhd, Kuala Lumpur, Malaysia) and controlled via a MyRio control board (MyRio, National Instruments, Mopac, Expwy Austin, U.S.A). The electromagnetic coils are fixed to upper and lower plastic frames to keep all magnetization axes parallel to each other. The electromagnetic configuration provides a planar footprint of 150 mm×150 mm and hight of 60 mm. A position sensing device (Leap Motion, San Francisco, CA, U.S.A) is fixed above the electromagnetic configuration at hight of 50 cm.

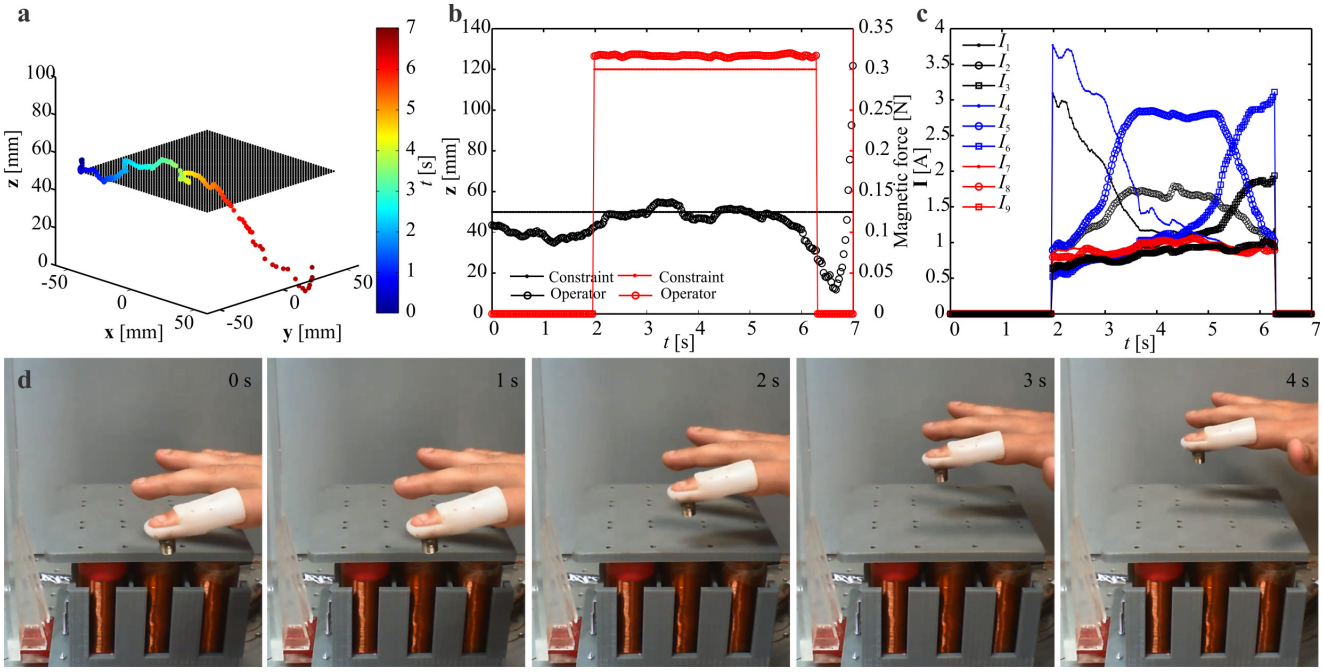

Fig. 4. A representative magnetic rendering of a flat surface (at height of 50 mm) shows the position of the operator and the calculated forces and currents during shape differentiation. (a) The constraint ($g(\mathbf{r}, t)$) of the flat surface is decomposed into 3721 points (small black circles). The trajectory of the finger splint indicates a deviation from the rendered flat surface only outside the workspace of the system. (b) The position of the finger splint along **z**-axis indicates maximum deviation of 14 mm from the flat surface during this trial. At time, $t = 6$ second, the participant moves outside the workspace of the system. (c) Current inputs are calculated and supplied to the electromagnetic coils based on the position of the wearable finger split during this trial. (d) The participant slides his finger on the surface several times. The successful participants differentiate the virtual flat surface from other objects in 92 seconds. *Please refer to the accompanying video.*

III. Sensing 3D Virtual Objects

We experimentally conduct a participant study to evaluate the ability of the system to render 3D objects.

A. Preliminary Validation of Rendering 3D Virtual Objects

Haptic rendering of a virtual 3D object is achieved by generating its constraint surface $g(\mathbf{r}, t)$ using SOLIDWORKS. The surface constraint is discretized into 3D points. This step is followed by calculation of the force constant λ by solving (9) using MATLAB's *fminmax* function. This optimization routine is performed only once for each object. The current input to the electromagnetic coils are calculated by solving (8) using MATLAB's *fmincon* function. Fig. 4(a) shows 3721 points that span a flat surface. This virtual surface has an edge length of 100 mm and is located at hight of 50 mm along **z**-axis. We allow a participant to explore the virtual flat surface without any prior information pertaining to the geometry of the object. Position of the wearable finger splint is measured and used to calculate the magnetic force, as shown in Fig. 4(b). A constraint force at each of these points is calculated using (10) with λ of 6 N/m (which exerts magnetic force of 0.3 N at height of 5 cm), as shown in Fig. 4(b). In this representative trial, the maximum deviation between the wearable finger splint and the reference surface is 14 mm (at time $t \approx 1$ seconds). At time $t \approx 6$ seconds, the participant moves outside the workspace of the system, and this action is repeated by each participant to differentiate between 3D objects. Fig. 4(c) shows the input currents to the electromagnetic coils in this representative trial. *Please refer to the accompanying video.*

B. Participant Study and Statistical Analysis

We conduct a participant study to validate the ability of our electromagnetic-based haptic interface and the impedance-type haptic algorithm to render 3D virtual objects. Observations of ten participants with an average age of 23 are collected. Each participant is allowed to distinguish between four 3D virtual objects, i.e., flat surface, half-sphere, half-cylinder, and wedge. The number of trials is limited to 16 trials and this experiment is repeated 4 times for each virtual object using our impedance-type haptic algorithm (Case I) and in the absence of position feedback (Case II). At the end of each trial, participants are asked to provide their observation. The result of each trial is not provided to the participant. All participants use the electromagnetic-based haptic interface for the first time and they are not involved again. In each trial, we measure the position of the finger during interaction, exerted magnetic forces, and input currents to the electromagnetic coils, as shown in Fig. 4.

Fig. 5(a) shows the representative results of the impedance-type haptic algorithm for the mentioned four objects. We observe that participants differentiate between the objects in approximately 79 ± 21 seconds ($n = 160$) although the time of each trial is not limited. The successful and unsuccessful trials for each participant are shown in Fig. 5(a) using the filled and empty markers, respectively.

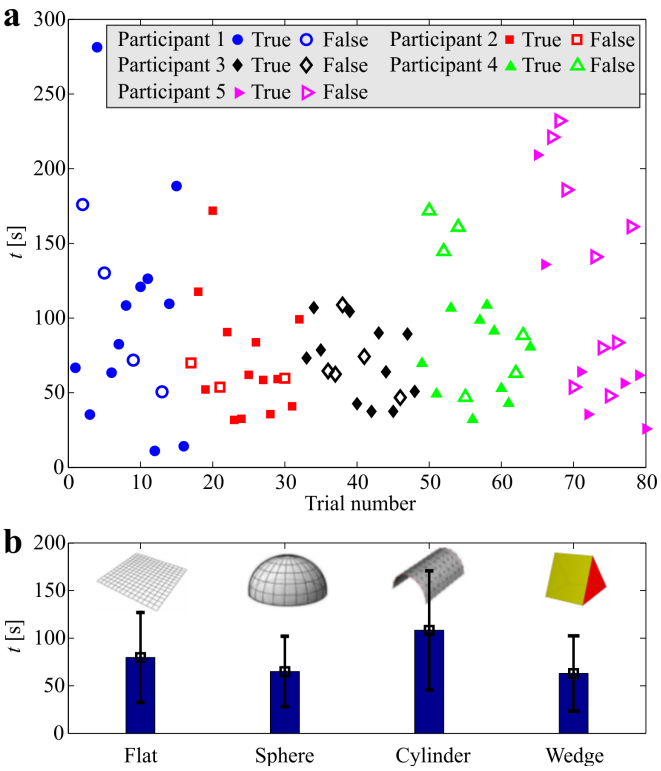

Fig. 5. The observations of 5 representative participants indicate their ability to differentiate between 4 virtual shapes (flat, half-sphere, half-cylinder, and wedge). Each participant is allowed to distinguish between the objects for 16 trials only. Our system renders the objects in a random order and the result of each observation is not provided to the participant after each trial. (a) The filled and empty markers indicate the successful and unsuccessful trials, respectively. (b) Participants spent relatively short time in making successful observations for the virtual sphere and wedge, as opposed to the virtual flat surface and half-cylinder.

Fig. 5(b) shows the average time taken by the ten participants for each object. For the virtual half-cylinder, participants spend 108.2 ± 62 seconds $(n = 160)$ and achieve success rate of 60% in their observations. The observation time is decreased to 79.6 ± 47.3 seconds $(n = 160)$ for the virtual flat surface and the success rate is increased to 62.5%. For the virtual sphere and wedge, the average observation time is measured as 64.9 ± 36.9 seconds $(n = 160)$ and 64 ± 45 seconds $(n = 160)$ with success rate of 67.5% and 77.5%, respectively. Therefore, the average success rate of the participants using the impedance-type haptic algorithm is $66.87 \pm 14.4\%$ $(n = 160)$.

Although our impedance-type haptic algorithm is based on position feedback, it is also possible to explore a virtual object using static magnetic forces [9]. These forces are calculated using (8) to minimize the force error (7) regardless to the position of the participant. We repeat the previous trials using the same participants without position feedback, as shown in Table I. In this case, the success rate in distinguishing between the four virtual objects is decreased to $55.15 \pm 15.8\%$ $(n = 160)$. To understand the significance of position feedback, we devise the following null (H_0) and alternative (H_a) hypothesis (confidence level of 90%):

TABLE I

EXPERIMENTAL RESULTS OF THE MAGNETIC RENDERING OF 4 REPRESENTATIVE THREE-DIMENSIONAL (3D) VIRTUAL OBJECTS, I.E., FLAT SURFACE, HALF-SPHERE, HALF-CYLINDER, AND WEDGE. TEN PARTICIPANTS EXPERIMENTALLY DEMONSTRATE $66.87 \pm 15.0\%$ SUCCESS RATE $(n = 160)$ IN DISTINGUISHING THE FOUR 3D GEOMETRIES USING THE IMPEDANCE-TYPE HAPTIC RENDERING ALGORITHM. IN THE ABSECNE OF POSITION FEEDBACK, THE SUCCESS RATE IS $55.15 \pm 15.8\%$.

Object				
1	1.0 (0.75)	0.75 (0.5)	0.25 (0.5)	1.0 (1.0)
2	0.75 (0.5)	0.75 (0.5)	0.75 (0.75)	1.0 (1.0)
3	0.75 (0.75)	0.75 (0.75)	0.25 (0.25)	1.0 (0.75)
4	0.50 (0.5)	0.75 (0.75)	0.50 (0.25)	0.75 (0.5)
5	0.5 (0.5)	0.5 (0.0)	0.25 (0.0)	0.5 (0.75)
6	0.0 (0.75)	0.5 (1.0)	0.75 (0.5)	0.5 (0.5)
7	0.5 (0.75)	0.75 (0.75)	0.75 (0.75)	0.5 (0.75)
8	1.0 (0.75)	1.0 (0.5)	0.75 (0.5)	0.75 (0.25)
9	0.5 (0.5)	0.25 (0.5)	0.75 (0.25)	0.75 (0.25)
10	0.75 (0.25)	0.75 (0.25)	1.0 (0.75)	0.75 (0.25)

- H_0: Success rate for Case I is less than that of Case II;
- H_a: Success rate for Case I is greater than Case II;

Fig. 6(a) shows the number of successful trials for each participant in Case I (impedance-type haptic rendering) and Case II (rendering without position feedback). The observations are examined using Paired T-Test. First, we test the normality of the two groups of data using Shapiro-Wilk test of normality. We conclude that the two groups of data are normally distributed. Second, the Paired T-Test suggests p-value $= 0.052 < \alpha$. Therefore, we reject the null hypothesis and accept the alternative hypothesis, and hence there is a statistical evidence to conclude that the mean success rate for the Case I is greater than the mean success rate for Case II, at $\alpha = 0.1$ and 90% confidence level.

Our experimental results show that participants achieve success rate of 66.87% using the impedance-type rendering algorithm. This success rate is decreased to 55.15% for rendering 3D object without position feedback. Our analysis shows that there is a statistical evidence to conclude that the mean success rate for Case I is greater than that of Case II, at $\alpha = 0.1$ and 90% confidence level. The incorporation of position feedback has additional benefits such as the capability of rendering relatively complex virtual objects and the utilization of lower current input owing to the activation of less number of coils based on the position of the wearable finger splint. However, the success rate is limited owing to the confusion between specific virtual objects during the experiments. We construct the confusion matrix [12] to show the predicted shapes (row) by the participants against the actual shapes (column). Table II shows the shapes that confuse the participants during the experiments while using our impedance-type rendering algorithm. Confusion between objects is observed in 15 trials between the flat surface and half-cylinder and in 13 trials between half-sphere and half-cylinder. Our measurements also show that the flat surface

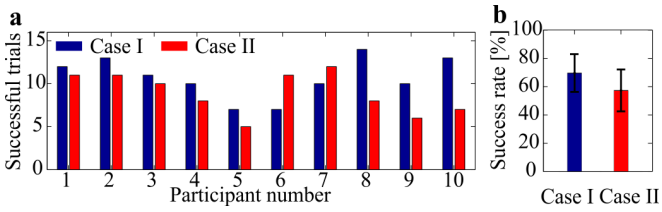

Fig. 6. The ability of the participants to distinguish between the virtual geometries is enhanced by the incorporation of position feedback. (a) Measurements are collected from the observation of 10 participants using position feedback (Case I) and without (Case II) position feedback. (b) The impedance-type haptic interface enables participants to distinguish objects with 66.87% success rate, whereas exploring the virtual objects without position feedback achieves success rate of 55.15%. The means and standard deviations are calculated using 16 trial for each 10 participant in each case.

and half-sphere are confused in 11 trials, whereas the flat surface and wedge are confused in 10 trials. Table II shows that the participants are confused between the wedge and the half-sphere or the half-cylinder in 4 trials. In the absence of position feedback (observations between brackets), participants are confused most in differentiating between the virtual flat surface and the half-sphere in 12 trials, and the half-sphere and -cylinder in 16 trials. Participants are also confused between the flat surface and half-sphere in 12 trials, and similarly, the virtual wedge and half-sphere and -cylinder are confused in 16 trials by all participants. Therefore, the incorporation of position feedback in the design of the impedance-type haptic algorithm decreases the confusion between virtual objects based on the observation of the participants.

IV. Conclusions and Future Work

An electromagnetic-based haptic interface is designed, developed, and verified using observations of participants. This system is based on an impedance-type haptic rendering algorithm that provides a controlled magnetic force on a permanent magnet attached to a wearable orthopedic finger splint. The controlled magnetic force enables the participants to perceive 3D virtual objects in mid-air. The capability of the system to render 3D virtual objects is evaluated in the presence and absence of position feedback. Our experimental results show that participants distinguish between the geometry of four 3D objects with success rate of 66.8% while using position feedback and 55.15% in the absence position feedback. Our analysis shows a statistical evidence to conclude that the mean success rate for Case I is greater than that of Case II, at $\alpha = 0.1$ and 90% confidence level.

As part of future studies, we will adapt our impedance-type rendering algorithm to incorporate multiple dipole moments to improve the perception of the participants during the interaction with virtual objects. The success rate of our system is limited owing to the dependence of our rendering algorithm on a single magnetic force. The incorporation of multiple magnetic dipoles will enable us to exert several controlled magnetic forces on specific locations within a wearable device, and as a consequence, the success rate in object differentiation will be improved. In addition, a head-mounted display will be integrated to our electromagnetic-based haptic interface to deploy virtual images of the 3D object over other real-world objects.

TABLE II

Confusion matrix shows the predicted objects (row) versus the actual objects (column) for the impedance-type haptic interface ($n = 160$) and for rendering virtual objects without position feedback ($n = 160$). Measurements of the second case is shown between brackets.

Object				
	25 (**24**)	5 (4)	8 (15)	8 (5)
	6 (8)	**27** (**22**)	7 (5)	0 (8)
	7 (6)	6 (11)	**24** (**18**)	1 (3)
	2 (2)	2 (3)	1 (2)	**31** (**24**)

References

[1] N. Magnenat-Thalmann and U. Bonanni, "Haptics in virtual reality and multimedia," *IEEE Transaction on Multimedia*, vol. 13, no. 3, pp. 6–11, August 2006.

[2] G. C. Burdea, "Haptic feedback for virtual reality," *Virtual Reality and Prototyping Workshop*, Laval, France, June 1999.

[3] K. Salisbury, F. Conti, and F. Barbagli, "Haptic rendering: introductory concepts," *IEEE Computer Graphics and Applications*, vol. 24, no. 2, pp. 24–32, March 2004.

[4] Carlos Bermejo and Pan Hui, "A survey on haptic technologies for mobile augmented reality," *arXiv:1709.00698v3*, September 2017.

[5] T. Iwamoto, M. Tatezono, T. Hoshi, and H. Shinoda, "Airborne ultrasound tactile display," in *Proceedings of the International Conference and Exhibition on Computer Graphics and Interactive Techniques*, pp. 1-1, Los Angeles, California, August 2008.

[6] Y. Suzuki and M. Kobayashi, "Air jet driven force feedback in virtual reality," *IEEE Transactions on Computer Graphics and Applications,* vol. 25, no. 1, pp. 44–47, January 2005.

[7] S. Gupta, D. Morris, S. N. Patel, and D. Tan, "Airwave: Noncontact haptic feedback using air vortex rings," in *Proceedings of ACM International Joint Conference on Pervasive and Ubiquitous Computing*, pp. 419–428, Zurich, Switzerland, September 2013.

[8] Q. Zhang, H. Dong, and A. El Saddik, "Magnetic field control for haptic display: system design and simulation," *IEEE Access*, vol. 4, pp. 299–311, January 2016.

[9] A. Adel, M. Abou Seif, G. Hölzl, M. Kranz, S. Abdennadher, and I. S. M. Khalil, "Rendering 3D virtual objects in mid-air using controlled magnetic fields," in *Proceedings of the IEEE International Conference on Intelligent Robots and Systems (IROS)*, pp. 349–356, Vancouver, BC, Canada, September 2017.

[10] M. P. Kummer, J. J. Abbott, B. E. Kartochvil, R. Borer, A. Sengul, and B. J. Nelson, "OctoMag: an electromagnetic system for 5-DOF wireless micromanipulation," *IEEE Transactions on Robotics*, vol. 26, no. 6, pp. 1006–1017, December 2010.

[11] I. S. M. Khalil, L. Abelmann, and S. Misra, "Magnetic-based motion control of paramagnetic microparticles with disturbance compensation," *IEEE Transactions on Magnetics*, vol. 50, no. 10 (5400110), October 2014.

[12] B. Long, S. A. Seah, T. Carter, and S. Subramanian, "Rendering volumetric haptic shapes in mid-air using ultrasound," *ACM Transactions on Graphics*, vol. 33, no. 6, pp. 181(1–10), November 2014.